
PERGAMON

Journal of Quantitative Spectroscopy & Radiative Transfer 81 (2003) 107–115

Journal of Quantitative Spectroscopy & Radiative Transfer

www.elsevier.com/locate/jqsrt

FLYCHK: an extension to the K-shell spectroscopy kinetics model FLY

H.-K. Chung[a,*], W.L. Morgan[b], R.W. Lee[a]

[a] *Lawrence Livermore National Laboratory, P.O. Box 808, L-399, Livermore, CA 94550, USA*
[b] *Kinema Research, P.O. Box 1147, Monument, CO 80132, USA*

Accepted 15 February 2003

Abstract

The K-shell spectroscopy code FLY and its predecessors have been employed to study hot dense plasmas for decades. FLY has provided a basis for studies of K-shell ions up to $Z = 26$, where its ease of use, PC application base, and synthetic spectral production have made it attractive to both experimentalists and modelers. However, the application has been focused on K-shell ions where less ionized species are represented as a ground state only. To attempt to make this simple model predict the ionization and recombination through the less ionized stages, we extend the model to include kinetics models for all ion stages. The emphasis of this extension is not to provide detailed spectra or population for the L- or M-shell, but to provide a K-shell model with enhanced accuracy in those cases where ionization and recombination through the L- and M-shell are important. This work is a first step in generating an application that will allow detailed analysis of sub-picosecond self-consistent velocity distribution and population kinetics solutions. We will discuss the extensions and provide examples. Finally, we will outline the progress towards the eventual goal of the self-consistent solution.

Keywords: Collisional-radiative modeling; Hydrogenic mode; K-shell spectroscopy

1. Introduction

K-shell spectroscopy is a powerful tool to understand hot dense plasmas since K-shell ions are present over a wide range of plasma conditions due to their large ionization potentials. The K-shell spectroscopy code suite FLY has served as a useful and reliable tool to understand kinetics and X-ray spectra of highly ionized plasmas. [1] It uses highly accurate atomic data for K-shell ions and Li-like ions whose populations are calculated from rate equations including all relevant collisional

* Corresponding author.
E-mail address: hchung@llnl.gov (H.-K. Chung).

0022-4073/03/$ - see front matter © 2003 Elsevier Science Ltd. All rights reserved.
doi:10.1016/S0022-4073(03)00064-5

and radiative processes. It is capable of performing calculations for steady-state or time-dependent cases as well as radiation-dominated cases. Attractive features of the code FLY include an easy-to-use interface, portability to most PCs and Macs, graphics tools to plot line ratios and synthetic spectra for on-line analysis of X-ray measured data. The code has been validated and benchmarked over the past two decades by numerous experiments generating highly ionized plasmas such as laser-produced plasma or radiatively driven implosion experiments.

Although FLY has been used successfully, species less ionized than Li-like are represented by a single ground state and hence the accuracy will decrease when L- and M-shell ions start to play a dominant role either in the evolution toward the K-shell or are themselves major contributors to the ionization balance. Therefore, to improve the accuracy in those cases when ionization and recombination through the L- and M-shell are important, an extension is required to include excited levels as well as the ground state for L- and M-shell ions.

The extension to include the kinetics of L- and M-shell ions will make FLY applicable to plasmas that are colder and/or less ionized. Current applications of the extended code would include the study of relaxation processes of plasmas produced by high-intensity short pulse lasers where hot electron heating dominated the plasma production or high current density particle beams. In the future the X-ray free-electron lasers (XFEL) scheduled to operate in a few years will have a capability of focusing 10^{12}–10^{14} photons onto samples with pulse lengths of ~ 200 fs. The XFEL will be used in a wide range of applications including studies of biology, material structure, warm and hot dense matter. However, to characterize the sample on the time scales of the plasma formation, one will need to model the evolution of ionization distributions on the order of femtoseconds. It is our goal to make the extended version of FLY general and portable and eventually available for researchers interested in studying highly non-equilibrium states of hot and warm dense matter.

In order to make the atomic model general while maintaining the computational efficiency, a screened hydrogenic model is applied to describe the ground and excited states of L- and M-shell ions including inner-shell excited states. The details of this extension are described in Section 2 and we provide examples of the improvements in Section 3. Finally, we report on the code performance by studying the relaxation of population distributions after initial inner-shell photoionization occurs.

2. Kinetics model

In the extended version, named FLYCHK, three different atomic models are implemented and users are able to choose a model based on the application of interest in the following ways;

- detailed model for K-shell and Li-like ions and the ground states for all the other ions, this is the original FLY code;
- detailed model for K-shell and Li-like ions as in the original code FLY, with a hydrogenic model for selected ions and the ground states for the remaining ions;
- hydrogenic model for all ions including K-shell ions.

The detailed model for K-shell and Li-like ions can be found in Ref. [1] and only the hydrogenic model based on the work presented in Ref. [2] is described in this section.

2.1. Energy levels

Each hydrogenic level for each ionization stage i is described by the principal number of n. The ionization potential of an excited level with an outermost bound electron of principal quantum number n is computed using the hydrogenic approximation with relativistic corrections

$$I_n = Q_n^2 e^2/(2a_0 n^2)(1 + (\alpha Q_n/n)^2(2n/(n+1) - 3/4)), \tag{1}$$

where Q_n is the screened charge, a_0 Bohr radius and $e^2/2a_0$ is Rydberg energy. The screened charge is defined using the screening constants [2,3] as

$$Q_n = Z_n - \sum_{m<n} \sigma(n,m)P_m - 0.5\,\sigma(n,n)(P_n - 1), \tag{2}$$

where P_n is the occupation number of the level n. For accuracy and consistency with the existing FLY, we use the empirical ionization energies for the ground states [4].

Autoionizing inner-shell excited levels are included in the hydrogenic approximation. The energy of the first inner-shell excited level with respect to the ground state of an ionization stage is obtained as the difference between the ionization energy of the inner-shell electron and that of the ground state of the next ionization stage. The higher-lying inner-shell excited levels with an n-shell electron promoted from the first inner-shell excited level are sequentially constructed by adding the energy of the bound n-shell excited level with respect to its ground state to the energy of the first inner-shell excited level. There is an energy shift required for these inner-shell excited levels to ensure that these lie below their continuum limit. For the K-shell excited levels, the shift is the difference between the $n = 2$ energy level of He-like ions with respect to the ground state and the ionization energy difference of $n = 1$ and 2 levels of Li-like ions. For the L-shell excited levels, the shift is derived, e.g., from the difference involving $n = 3$ energy level of Ne-like ions and the ionization energy difference of $n = 2$ and 3 levels of Na-like ions.

2.2. Radiative processes

An absorption oscillator strength of a transition from a level n to a level m is defined with hydrogenic oscillator strength $f^{\mathrm{H}}(n \to m)$

$$f(n \to m) = f^{\mathrm{H}}(n \to m)P_n, \tag{3}$$

where P_n is the occupation number of level n. The oscillator strength together with Einstein's relation are used to generate the spontaneous and stimulated emission rates and absorption coefficient for radiative bound–bound transitions. For bound-free processes, Kramers' quasi-classical photoionization cross-sections are used [5].

$$\sigma(E) = \frac{64\pi\alpha a_0^2}{3^{1.5}} \frac{I_n^{2.5} I_{\mathrm{H}}^{0.5}}{Q_n E^3}, \tag{4}$$

where α is fine-structure constant and I_n is the ionization potential of the n shell and I_{H} is Rydberg energy. Using detailed balance and photoionization rate coefficients, we generate the spontaneous radiative recombination rate coefficients, which in unit of $(\mathrm{cm}^3/\mathrm{s})$ is written as a function of electron

temperature T_e in eV as

$$R = 1.917 \times 10^{-15} \frac{g_i}{g_k} \frac{I_n^{2.5}}{T_e^{1.5} Z} \exp\left[\frac{I_n}{T_e}\right] E_1\left[\frac{I_n}{T_e}\right], \tag{5}$$

where g_i and g_k are statistical weights of the initial state and the state into which the recombination occurs, respectively, and E_1 is the exponential integral.

2.3. Collisional processes

We use collisional excitation cross-sections based on oscillator strength for the allowed transitions [6]

$$\sigma_{ij}(U) = 4\pi a_0^2 (2\pi/\sqrt{3})(E_H/E_{ij})^2 f_{ij} g U^{-1}, \tag{6}$$

where $U = E/E_{ij}$, E is the initial electron energy, E_H is the hydrogen ionization energy, f_{ij} is the absorption oscillator strength and g is the effective gaunt factor. We use the gaunt factor suggested by Mewe [7]

$$g(U) = A + BU^{-1} + CU^{-2} + D \ln U, \tag{7}$$

where $A = 0.15$, $B = C = 0$ and $D = 0.28$. The rate coefficients are computed in unit of cm^3/s by integrating the cross-sections over the Maxwellian electron energy distribution as

$$R(T_e) = 1.578 \times 10^{-5} T_e^{-1/2} E_{ij}^{-1} f_{ij} \bar{g}(y) \exp(-y), \tag{8}$$

where $y = E_{ij}/T_e$, E_{ij} and T_e are in eV and

$$\bar{g}(y) = A + (By - Cy^2 + D) e^y E_1(y) + Cy. \tag{9}$$

The same formalism is used for inner-shell excitation processes.

A semi-empirical formula of Burgess and Chidichimo [8] is used for collisional ionization from a level n,

$$\sigma_n(E) = \pi a_0^2 C P_n (E_H/I_n)^2 (I_n/E) \ln(E/I_n) W(E/I_n), \tag{10}$$

where for $E > I_n$

$$W(E/I_n) = [\ln(E/I_n)]^{\beta I_n/E}, \tag{11}$$

where

$$\beta = 0.25[(100z + 91)/(4z + 3)]^{1/2} - 5) \tag{12}$$

and z is the charge of the ion. For $E \leqslant I_n$, $W(E/I_n) = 0$.

Note that for the constant C, we use the suggested value 2.3 [8] while it is 2.77 in the Lotz formula [9]. The rate coefficient is written as

$$R(T_e) = 2.1715 \times 10^{-8} C P_n (I_H/I_n)^{3/2} (I_n/T_e)^{1/2} E_1(I_n/T_e) w(I_n/T_e), \tag{13}$$

where

$$w(I_n/T_e) = [\ln(1 + T_e/I_n)]^{\beta/(1+T_e/I_n)}. \tag{14}$$

2.4. Inner-shell processes

The two processes involving inner-shell excited levels, autoionization and inner-shell photoionization, are implemented with atomic data generated by *jj* configuration average codes. K- and L-shell photoionization cross-sections are computed for hydrogenic levels by using Hartree–Fock–Slater wave functions [10,11]. Autoionization rates are included for KLn(and LMn) transitions and these rates are calculated by perturbation theory in the Dirac–Hartree–Slater approach [12,13].

Dielectronic recombination processes are included via electron capture processes, whose rates are determined by detailed balance. It should be noted, however, that due to the hydrogenic approximation, $\Delta n = 0$ transitions are not included and these contributions can be the dominant dielectronic recombination processes at low temperatures. Work is in progress to establish the uncertainty associated with the hydrogenic assumption.

3. Results

3.1. Improvement on ionization distributions

The extension to the L- and M-shell affects the ionization distribution most notably in the case of low-temperature and high-density plasmas. In these cases, three-body recombination is important since the rates are proportional to electron density squared. In particular, rate coefficients of three-body recombination increase with the principal quantum number as n^3 and hence the high-lying states act as recombination channels for high-density plasmas. Therefore, the excited states of L- and M-shell ions present in FLYCHK will lead to lower ionization states for high-density plasmas compared with the results of FLY that includes ground states for ions less ionized than Li-like. This is demonstrated in the following two examples.

The first example is the problem of a recombining carbon ion. Initially, the problem starts with fully stripped carbon at a temperature, T_e, of 2 eV and n_e of 10^{19} cm^{-3}. We calculate the time-dependent populations for fixed T_e and n_e. We compare the average charge states of three different models in Fig. 1. The first model, denoted FLY, uses detailed levels for H-, He- and Li-like ions while including only the ground states as in FLY. The second model, denoted FLYCHK, uses the hydrogenic levels in FLYCHK for Be, B and C ions. The third model, denoted FLYCHK-HY, uses the hydrogenic model for all ions. The time-dependent average charge state can be seen to decrease faster in FLYCHK than in FLY-like model. The recombination to the Li-like ions accelerates approximately at 10 ps due to high three-body recombination rates to the excited states in FLYCHK.

Next, we can examine the role of detailed levels in this problem by comparing the FLYCHK-HY and FLYCHK models. Here, we can see that the hydrogenic approximation for the He-like levels leads to even faster recombination. It is found that the metastable states of He-like ions slow the downward cascades from the upper levels to the ground state and eventually slow the overall recombination processes. It should be noted that the substantial differences between FLYCHK-HY and FLYCHK are primarily due to the somewhat unphysical nature of the time-dependence of the problem and the differences are substantially smaller in most steady-state problems tested. Nevertheless, one should be advised of the effects of hydrogenic approximations and associated uncertainties in the determination of ionization distributions.

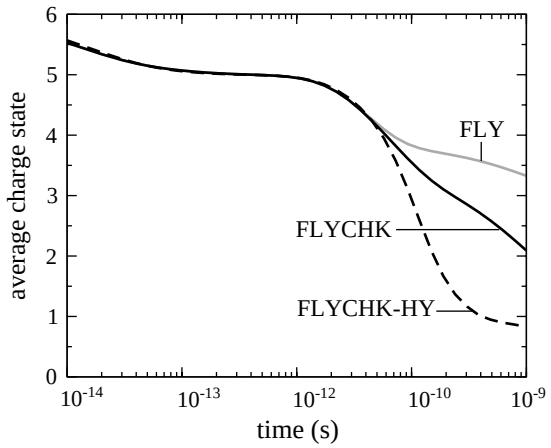

Fig. 1. Average charge states of three different models are compared for the case of the carbon plasma recombining from the fully stripped ions at 2 eV.

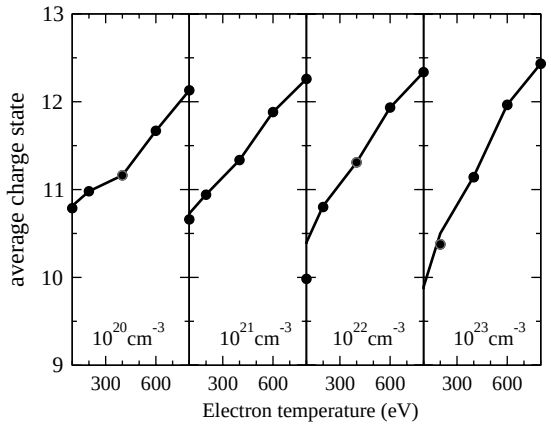

Fig. 2. Average charge states at four different electron densities show that the excited states of L-shell ions can make a significant change in the ionization distributions of the high electron density plasmas.

The next example concerns the steady-state ionization distributions of aluminum ions as a function of T_e and n_e. The average charge state calculated by the FLY model and the FLYCHK model are compared in Fig. 2 at T_e of 100, 200, 400, 600 and 800 eV and n_e of 10^{20}, 10^{21}, 10^{22}, and 10^{23} cm^{-3}. For a given density, the average charge state increases as a function of T_e. For a given T_e, say, 600 eV, the average charge states increase as a function of n_e if the plasma state changes from the coronal state to collisional-radiative regime. On the other hand, for a low T_e, say, 100 eV, the average charge state decreases as a function of n_e since the three-body recombination processes become significant as the plasma goes to the LTE limit. As in the first example, FLYCHK produces lower ionization states when three-body recombination through high-lying states becomes important at low temperatures and high densities.

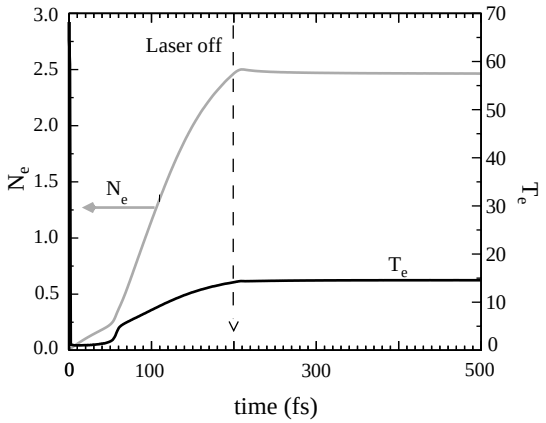

Fig. 3. Time-dependent electron density and temperature distributions of aluminum ions during and after the intense irradiation.

3.2. Application to near-neutral plasmas

Recent advances in laser and beam technology have led to the generation of near-neutral plasmas with low temperatures of a few eV and near-solid density. Plasma states of such warm dense matter are not very well understood [14] and there is a growing interest in plasma, condense-matter and statistical physics communities. It is our goal to apply the L- and M-shell model in FLYCHK to study warm dense plasmas as well as hot dense plasmas. Here, we show that FLYCHK is a potential tool to study population relaxation and ionization distributions of such plasmas.

As the first step, we study the time-dependent ionization distributions of aluminum ions in the warm dense regime. Here a 20 μm thick solid Al target is illuminated by a 200 fs pulse with 10^{12} photons each of 200 eV, a case relevant to the XUV-FEL at DESY [15]. In the present work, we make a series of assumptions to study and validate the population relaxation processes for near-neutral systems contained in FLYCHK. For example, we assume that the target remains at solid density while assuming that the band structure of solid aluminum with three free electrons does not play a role and initially all the atoms are neutral. We also assume the instantaneous thermalization of electrons and hence the energy density, E, of electrons is distributed according to $E = \frac{3}{2} n_e T_e$. The energy balance is obtained from the electron kinetic energy and internal energy of ions, which will equal the energy deposited by laser less than the energy radiated away by spontaneous decay. The n_e and the ion internal energy are calculated self-consistently from the time-dependent population distribution.

In this problem, we would like to investigate autoionization and electron capture processes as well as collisional and radiative relaxation processes upon photo-ionization by the high-energy photons. The calculated temperature T_e as a function of time shown in Fig. 3 indicates that population relaxation processes operate in FLYCHK as intended. Initially, T_e corresponds to the energy of the ejected electron. As electrons are liberated by Auger processes and collisional ionization occurs, T_e decreases rapidly as the energy deposited by laser is distributed to electron kinetic energy and the internal energy of ions. While the internal energy rises as excited and ionized levels are populated

from the ground state by electron collisions, the levels also reach collisional equilibrium and hence the growth rate of internal energy slows down. Then T_e rises since more of the energy deposited in ion internal energy is passed to electron kinetic energy. By the time the photon source is off, T_e has reached 15 eV and the system remains steady. The temperature reached at the end of the pulse agrees with the energy balance between an independently calculated value of the total energy deposited during the irradiation and the internal energy of a LTE plasma at that time. This indicates that the inner-shell ionization energy deposition model in FLYCHK is, at least, reasonable and the population distributions correctly reach the equilibrium value.

4. Future work

In this paper, we summarized the L- and M-shell model in FLYCHK using the hydrogenic approximation and showed the improvement of ionization balance for K-shell dominated plasmas. As a next step, we plan on conducting comparisons of ionization distributions for the L-shell dominated plasmas between the hydrogenic model and a detailed model. We also plan to investigate the possibility of generating complex spectra from the simple hydrogenic model.

For a realistic model of XFEL heating of aluminum target, we need an initial condition for our model and the capability to obtain electron energy distributions. For the initial condition for our model, one should address the interaction of the inner-shell liberated electrons with the solid aluminum and the ionization of secondary electrons liberated upon high-intensity X-ray photons. At the early phase of irradiation, the electron distribution is expected to be highly non-equilibrium, which will converge to Maxwellian distribution with time. Such non-Maxwellians should be consistent with the population distributions in the plasmas. Work is currently underway to implement a Boltzmann solver for electron energy distribution.

Acknowledgements

The authors thank J. Scofield and M. Chen for their generous help. This work was performed under the auspices of the US Department of Energy by University of California Lawrence Livermore National Laboratory under Contract No. W-7406-Eng-48.

References

[1] Lee RW, Larsen JT. JQSRT 1996;56:535.
[2] Lee YT. JQSRT 1987;38:131.
[3] Marchand R, Caille S, Lee YT. JQSRT 1990;43:149.
[4] Kelly RL, Palumbo LJ. Technical report no. NRL-7599, NRL Report, 1973.
[5] Kramers H. Philos Mag 1923;46:836.
[6] Van Regemorter H. Ap J 1962;136:906.
[7] Mewe R. Astron Astrophys 1972;20:215.
[8] Burgess A, Chidichimo MC. Mon Not R Astron Soc 1983;203:1269.
[9] Lotz W. Z Phys 1967;206:205.
[10] Scofield JH. Phys Rev A 1989;40:3054.

[11] Saloman EB, Hubbell JH, Scofield JH. At Data Nucl Data Tables 1988;38:1.
[12] Chen M, Laiman E, Crasemann B, Aoyagi M, Mark H. Phys Rev A 1979;19:2253.
[13] Perkins S, Cullen D, Chen M, Hubbel J, Rathkopf J, Scofield JH. Technical report no. UCRL-50400 V.30, Lawrence Livermore National Laboratory, 1991.
[14] Lee RW, Baldis HA, Cauble RC, Landen OL, Wark JS, Ng A, Rose SJ, Lewis C, Riley D, Gauthier JC, Audebert P. AIP Conference Proceedings, vol. 581. New York: AIP, 2001. p. 45–58.
[15] See the website http://www-hasylab.desy.de/facility/fel/ for information on the TESLA facility and the TESLA Test Facility (TTF) a soft X-ray FEL facility.